Fortuitously Superimposed Lattice Plane Secondary Diffraction from Crystalline Colloidal Arrays

Lei Liu, Pusheng Li, and Sanford A. Asher*

Contribution from the Department of Chemistry, University of Pittsburgh, Pittsburgh, Pennsylvania 15260

Received November 8, 1996[⊗]

Abstract: Dispersions of monodisperse macroionic spherical particles self assemble into bcc or fcc crystalline colloidal arrays (CCA), which efficiently Bragg diffract light in the near-IR, visible, and UV spectral regions, depending on the lattice constant and the crystal structure. We report here the observation of an anomalously intense "secondary diffraction", which occurs at half the wavelength ($\lambda^B/2$) of light diffracted by the lattice planes with highest particle density (the bcc (110) or the fcc (111) planes). This diffraction is >10-fold more intense than the primary diffraction at λ^B, and is narrow for light incident normal to the bcc (110) or the fcc (111) planes. This secondary diffraction results from fortuitously superimposed diffraction from numerous lattice planes oriented such that they diffract ca. $\lambda^B/2$ light. We quantitatively modeled the primary and secondary diffraction by using dynamical diffraction theory. This efficient diffraction phenomenon should be useful for optical device fabrication.

Introduction

Macroionic monodisperse colloidal spheres in aqueous solution can self assemble into three-dimensional periodic structures called crystalline colloidal arrays (CCA).[1−24] This self assembly, which minimizes the total electrostatic interparticle repulsion, causes the system to adopt either body-centered cubic (bcc) or face-centered cubic (fcc) structures, depending upon the interparticle interactions.[6,7,13−15] The CCA usually self assembles with the highest particle density planes (bcc (110) or fcc (111) planes) parallel to the container walls.[5−7,15−17]

These CCA resemble atomic and molecular crystals, but at a much larger scale. As a result, they strongly Bragg diffract UV, visible, and near-IR light.[4−17] Theoretical analysis using dynamical diffraction theory has successfully predicted the diffracted wavelength and bandwidth of fcc (111) plane diffraction for nonabsorbing, thick CCA, but the calculated extinction maxima were more than 40 times higher than the measured values.[18,19]

We report here extraordinarily intense diffraction from CCA for incident light at wavelength $\lambda^B/2$, normal to the bcc (110) or fcc (111) planes, when these planes show primary diffraction at λ^B. This "secondary diffraction" shows a 10- to 30-fold larger extinction than that of the primary diffraction. We demonstrate that this secondary diffraction results from numerous lattice planes which are fortuitously oriented to diffract $\lambda^B/2$ (*vide infra*). In addition, we have applied dynamical diffraction theory to model the primary and secondary extinction spectra of CCA diffraction. This efficient diffraction should be useful for high-efficiency narrow band rejection filters for spectroscopy,[8−12] display technology, and many pump-probe laser techniques.

Experimental Section

Monodisperse colloidal silica spheres were obtained from Nissan Chemical Industries, Ltd. (PST-1) as a 20% (by weight) aqueous suspension (pH = 8−10). The 101 nm diameter particles (relative standard deviation of 6.0%, as determined by TEM) have a surface charge of 0.26 μC/cm^2 (530 charges/particle, by conductivity titration). The suspension was ion-exchanged several times, after which strong diffraction was observed.

The silica CCA suspensions were injected between two quartz plates separated by 6.1 μm thick Mylar films. A Perkin-Elmer Lambda 9 UV/VIS/NIR spectrophotometer was used to measure the extinction spectra, and the incident beam was normal to the quartz cell surfaces.

* Address correspondence to this author.
⊗ Abstract published in *Advance ACS Abstracts,* February 15, 1997.
(1) Luck, W.; Klier, M.; Wesslau, H. *Ber. Bunsenges. Phys. Chem.* **1963**, *67*, 75−83.
(2) Hiltner, P. A.; Krieger, I. M. *J. Phys. Chem.* **1969**, *73*, 2386−2389.
(3) Davis, K. E.; Russel, W. B.; Glantschnig, W. J. *Science* **1989**, *245*, 507−510.
(4) Okubo, T. *J. Chem. Soc., Faraday Trans. 1* **1986**, *82*, 3185−3196.
(5) Monovoukas, Y.; Gast, A. P. *Langmuir* **1991**, *7*, 460−468.
(6) Carlson, R. J.; Asher, S. A. *Appl. Spectrosc.* **1984**, *38*, 297−304.
(7) Kesavamoorthy, R.; Tandon, S.; Xu, S.; Jagannathan, S.; Asher, S. A. *J. Colloid Interface Sci.* **1992**, *153*, 188−198.
(8) Asher, S. A. U.S. Patents 4,627,689, 4,632,517, 1986.
(9) Flaugh, P. L.; O'Donnell, S. E.; Asher, S. A. *Appl. Spectrosc.* **1984**, *38*, 847−850.
(10) Asher, S. A.; Flaugh, P. L.; Washinger, G. *Spectroscopy* **1986**, *1*, 26−31.
(11) Asher, S. A.; Holtz, J.; Liu, L.; Wu, Z. *J. Am. Chem. Soc.* **1994**, *116*, 4997−4998.
(12) Tse, A. S.; Wu, Z.; Asher, S. A. *Macromolecules* **1995**, *28*, 6533−6538.
(13) Sogami, I. S.; Yoshiyama, T. *Phase Transitions* **1990**, *21*, 171.
(14) Williams, R.; Crandell, R. S. *Phys. Lett.* **1974**, *48A*, 225−226.
(15) Clark, N. A.; Hurd, A. J.; Ackerson, B. J. *Nature* **1979**, *281*, 57−60.
(16) Monovoukas, Y.; Gast, A. P. *J. Colloid Interface Sci.* **1989**, *128*, 533−548.
(17) Kesavamoothy, R.; Rajalakshmi, M.; Babu Rao, C. *J. Phys: Condens. Matter* **1989**, *1*, 7149−7161.
(18) Spry, R. J.; Kosan, D. J. *Appl. Spectrosc.* **1986**, *40*, 782−784.
(19) Rundquist, P. A.; Photinos, P.; Jagannathan, S.; Asher, S. A. *J. Chem. Phys.* **1989**, *91*, 4932−4941.
(20) Zachariasen, W. H. *Theory of X-ray Diffraction in Crystals;* John Wiley and Sons: New York, 1946.
(21) Van Hulst, H. C. *Light Scattering by Small Particles;* John Wiley and Sons: New York, 1957.
(22) Bateman, J. B.; Weneck, E. J.; Eshler, D. C. *J. Colloid Sci.* **1959**, *14*, 308−329.
(23) Hiltner, P. A.; Papir, Y. S.; Krieger, I. M. *J. Phys. Chem.* **1971**, *75*, 1881−1886.
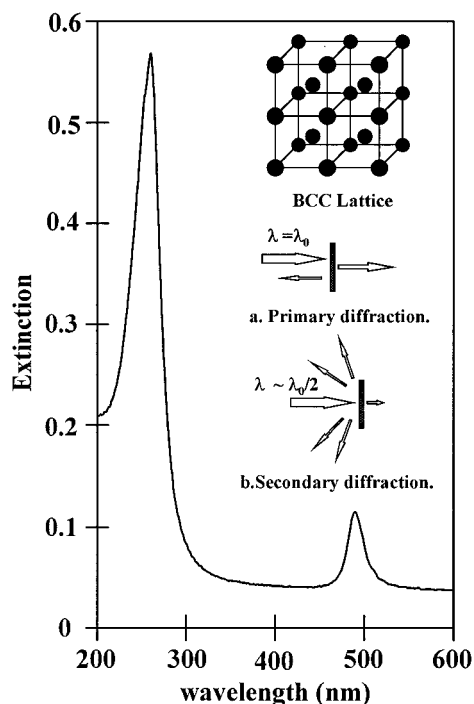(24) Colella, R. *Acta Crystallogr.* **1974**, *A30*, 413−423.

Figure 1. Extinction spectrum of a 6.1 μm thick silica CCA for light incident normal to the cell surface. The primary diffracted wavelength is 490 nm and the secondary diffracted wavelength is 260 nm. The insert shows the bcc lattice of a CCA and the diffraction from the primary and secondary lattice planes.

Results and Discussion

I. Superposition of Bragg Diffraction, Kinematical and Dynamical Predictions. The CCA normally self assembles with its highest particle density planes (the bcc (110) or fcc (111) planes) parallel to the quartz cell surfaces.[5-7,15-17] Figure 1 shows the extinction spectrum of a silica CCA. Two sharp extinction peaks are evident at ca. 490 and 260 nm. The 490-nm peak is the longest wavelength diffracted. It results from diffraction by either the bcc (110) or the fcc (111) planes.

This first-order "primary diffraction" almost follows Bragg's law.[18,19]

$$L\lambda^B = 2n_m d_{hkl} \sin\theta^B \qquad (1)$$

where L is the diffraction order, λ^B is the Bragg diffracted wavelength in air predicted by kinematical diffraction theory, n_m is the CCA average refractive index, d_{hkl} is the interplanar spacing of the lattice plane with Miller indices (hkl), and θ^B is the Bragg glancing angle of the incident beam relative to the (hkl) plane inside the crystal. d_{hkl} and the kinematical Bragg angle θ^B are easily calculated for light incident normal to the bcc (110) or fcc (111) lattice planes.[6]

A much more intense "secondary diffraction" occurs at $\lambda^B/2$ (Figure 1 and Table 3), which is far more efficient than that expected from second-order diffraction ($L = 2$). This strong ca. $\lambda^B/2$ diffraction results from diffraction from a set of lattice planes which are fortuitously oriented to fulfill the Bragg condition. For example, Tables 1 and 2 list the low index bcc and fcc planes and their diffraction wavelengths for light incident normal to the bcc (110) or fcc (111) planes; numerous planes diffract light at $\lambda^B/2$. Thus, if light is incident on the bcc or fcc crystal at a wavelength and angle where the bcc (110) or fcc (111) reciprocal lattice point lies on the Ewald reflection sphere at 180° from the origin of the reciprocal lattice, numerous reciprocal lattice points simultaneously lie on the $\lambda^B/2$ reflection

Table 1. Calculated Diffracted Wavelengths and Angles for a bcc Lattice[a]

h	k	l	d_{hkl} (nm)	θ^B (deg)	λ^B (nm)	λ^d (nm)
1	1	0	185.0	90	497	500
1	0	1	185.0	30	255	261
1	0	−1	185.0	30	255	261
0	1	1	185.0	30	255	261
0	1	−1	185.0	30	255	261
2	0	0	130.8	45	255	258
0	2	0	130.8	45	255	258
2	1	1	106.8	60	255	257
2	1	−1	106.8	60	255	257
1	2	1	106.8	60	255	257
1	2	−1	106.8	60	255	257
3	1	0	82.7	63.43	208	209
1	3	0	82.7	63.43	208	209
1	1	2	106.8	35.26	177	180
1	1	−2	106.8	35.26	177	180
2	2	2	75.5	54.74	177	178
2	2	−2	75.5	54.74	177	178
3	0	1	82.7	42.13	161	164
3	0	−1	82.7	42.13	161	164
0	3	1	82.7	42.13	161	164
0	3	−1	82.7	42.13	161	164
3	−1	0	82.7	26.57	116	120
1	−3	0	82.7	26.57	116	120
2	−1	1	106.8	16.78	101	111
2	−1	−1	106.8	16.78	101	111
1	−2	1	106.8	16.78	101	111
1	−2	−1	106.8	16.78	101	111
1	0	3	82.7	12.92	72	87
1	0	−3	82.7	12.92	72	87
0	1	3	82.7	12.92	72	87
0	1	−3	82.7	12.92	72	87

[a] h, k, l, Miller indices. d_{hkl}, interplanar spacing. θ^B, Bragg diffraction angle. λ^B, Bragg diffraction wavelenght. λ^d, dynamic diffraction wavelength.

Table 2. Calculated Diffracted Wavelengths and Angles for a fcc Lattice[a]

h	k	l	d_{hkl} (nm)	θ^B (deg)	λ^B (nm)	λ^d (nm)
1	1	1	184.8	90	497	500
2	0	0	160.0	35.26	255	260
0	2	0	160.0	35.26	255	260
0	0	2	160.0	35.26	255	260
2	2	0	113.2	54.74	255	258
2	0	2	113.2	54.74	255	258
0	2	2	113.2	54.74	255	258
3	1	1	96.5	60.5	233	236
1	3	1	96.5	60.5	233	236
1	1	3	96.5	60.5	233	236
1	1	−1	184.8	19.47	176	188
1	−1	1	184.8	19.47	176	188
1	−1	−1	184.8	19.47	176	188
3	1	−1	96.5	31.48	149	153
3	−1	1	96.5	31.48	149	153
1	3	−1	96.5	31.48	149	153
1	−1	3	96.5	31.48	149	153
1	−1	−3	96.5	31.48	149	153
1	−3	−1	96.5	31.48	149	153
3	−1	−1	96.5	10.02	68	95
1	1	−3	96.5	10.02	68	95
1	−3	1	96.5	10.2	68	95

[a] h, k, l, Miller indices. d_{hkl}, interplanar spacing. θ^B, Bragg diffraction angle. λ^B, Bragg diffraction wavelenght. λ^d, dynamic diffraction wavelength.

sphere (Tables 1 and 2). The deviation from exact $\lambda^B/2$ diffraction results from the dispersion of the refractive index, and from the dynamical diffraction correction to Bragg's law.

Kinematical diffraction theory, which leads to Bragg's law, neglects attenuation of the incident beam and assumes identical contributions from each lattice plane. In contrast, the CCA dif-

fraction follows dynamical diffraction theory (DDT), which considers coupling of the incident and diffracted waves due to the strong scattering. DDT predicts that the diffracted wavelength, λ^d, is[19,20]

$$\lambda^d = \lambda^B\left(1 - \frac{1-b}{4b\,\sin^2\theta^B}\psi_0\right) \qquad (2)$$

where b is the ratio of the direction cosines of the incident beam to the diffracted beam, which is -1, for normal incidence. ψ_0 measures the difference between the average refractive index of the CCA and the refractive index, n_w, of the solvent medium (water) surrounding the colloids:

$$\psi_0 = (n_m/n_w)^2 - 1 \qquad (3)$$

We utilized the known dispersion of the refractive index of water ($n_w(\lambda)$),[19,22] silica ($n_s(\lambda)$),[25] and the suspension medium ($n_m(\lambda)$):[19,23]

$$n_w = 1.324 + 3046/\lambda^2 \qquad (4)$$

$$n_s = 1.445 + 4158/\lambda^2 \qquad (5)$$

$$n_m = n_w + (n_s - n_w)\phi \qquad (6)$$

where λ is the wavelength of light in vacuum (nm) and ϕ is the volume fraction of the silica colloids.

Tables 1 and Table 2 list θ^B and λ^B for the planes which can diffract in the UV region when the primary diffraction occurs at 500 nm. We neglect planes with zero structure factors, where diffraction is forbidden,[6] and assume that no absorption occurs. For bcc, secondary diffraction at ca. 250 nm occurs from ten different diffracting planes (Table 1). The n_m increase from that at the primary diffraction wavelength causes a small red shift of the secondary diffraction from $\lambda^B/2$. The dynamical diffraction regime causes a further red shift due to the negative value of b; as a result, the diffractions from these planes are no longer perfectly superimposed. The secondary diffraction extinction splits into three bands at 261, 258, and 257 nm.

For fcc (Table 2), secondary diffraction occurs from six lattice planes at ca. $\lambda^B/2$. The DDT correction splits the diffraction into two bands at 260 and 258 nm.

The superposition of secondary diffraction occurs only for the extinction spectrum; the different lattice planes diffract light into widely different angles which approximately follow Bragg's law (Figure 1).

The degree of splitting of the secondary diffraction extinction spectrum depends upon the incident beam orientation. If the incident light is not normal to the bcc (110) or fcc (111) planes, the secondary diffracted wavelengths of the different lattice planes will differ, and the extinction spectrum will become complex and broaden (Figure 2). Obviously, the secondary diffraction extinction bandshape is very sensitive to the colloidal crystal misalignments and defects.

II. Dynamical Diffraction Theory Modeling of the Extinction Spectrum. We utilized dynamical X-ray diffraction theory[20] to calculate the ratio of the diffracted power (P_d) to the incident power (P_0) for nonabsorptive perfect crystals.

$$\frac{P_d}{P_0} = \frac{1}{y^2 + (y^2-1)\cot^2(A\sqrt{y^2-1})} \qquad \text{if } y > 1$$

(25) Weast, R. C. *Handbook of Chemistry and Physics*, 51st ed.; The Chemical Rubber Co.: Cleveland, Ohio, 51st edition, 1970; pp E-231.
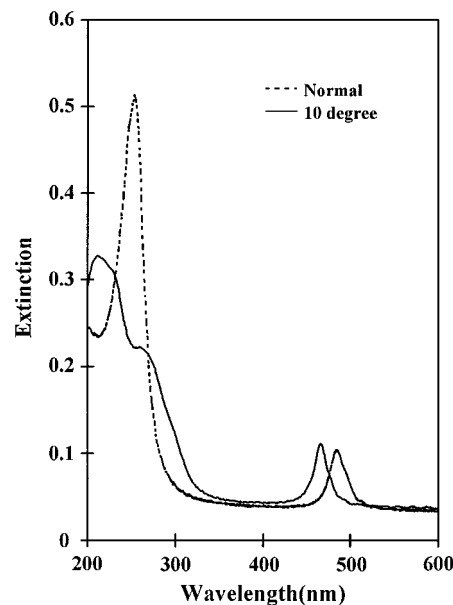

Figure 2. Crystal orientation dependence of the secondary diffraction extinction: (dashed line) light incident normal to the cell surface; (solid line) light incident 10° off of normal incidence.

$$\frac{P_d}{P_0} = \frac{1}{y^2 + (1-y^2)\coth^2(A\sqrt{1-y^2})} \qquad \text{if } y < 1$$

$$\frac{P_d}{P_0} = \frac{A^2}{A^2+1} \qquad \text{if } y = 1 \qquad (7)$$

For the extinction spectra (wavelength scale), y is solely a function of the incident wavelength λ:

$$y = \frac{\dfrac{1-b}{2}\psi_0 + 2b\dfrac{\lambda - \lambda^B}{\lambda^B}\sin^2\theta^B}{\sqrt{|b|}|\kappa\psi_H|} \qquad (8)$$

where κ is polarization factor, which is close to unity in our case (σ polarization). ψ_H is the Fourier transform of the refractive index modulation of the CCA lattice which, for our colloidal particles in the Rayleigh−Gans limit,[21] is given by:

$$\psi_H = C\left(\frac{d_{hkl}}{d}\right)^3\left[\frac{3(m^2-1)}{m^2+2}\right](\sin u - u\cos u) \qquad (9)$$

where $m = n_s/n_w$, C is equal to $3(3^{1/2})/8\pi^2$ and $1/(2^{1/2})\pi^2$ for bcc and fcc lattices, d is the nearest neighbor particle spacing, and u is the scattering size parameter:

$$u = \frac{2\pi n_m D_0 \sin\theta^B}{\lambda^B} \qquad (10)$$

where D_0 is the colloidal sphere diameter.

Quantity A can be expressed as:[18,20]:

$$A = \frac{\pi\kappa|\psi_H|}{\lambda^B}\frac{n_m}{n_0}\frac{t_0}{\sin\theta^B} \qquad (11)$$

where n_0 is the refractive index of air and t_0 is the penetration depth of the field along the normal to the crystal surface. As shown by Zachariasen,[20] the crystal is considered thick when $A \gg 1$, thin when $A \ll 1$, and intermediate when $\sim 0.4 < A <$

Table 3. Calculated and Observed Primary and Secondary Diffraction Efficiencies[a]

	primary			secondary			ratio
	λ^m_p	H_p	$\Delta\lambda_p$	λ^m_s	H_s	$\Delta\lambda_s$	H_s/H_p
measured	490	0.0778	20.0	260	0.531	39.5	6.9
	605	0.0138	22.3	312	0.206	38.1	14.9
	785	0.00255	20.0	397	0.0642	40.2	25.2
calculated							
bcc	490	0.0875	13.0	255	4.923	11.0	56.3
	605	0.0191	20.0	310	1.537	11.0	80.5
	785	0.00270	34.0	398	0.249	15.0	92.2
fcc	490	0.104	14.0	255	2.918	9.0	28.1
	605	0.0228	20.5	310	0.905	9.0	39.7
	785	0.00327	34.0	398	0.150	14.5	45.9

[a] λ^m_p, wavelength (nm, in air) for maximum extinction of primary diffraction. H_p, maximum extinction of primary diffraction. $\Delta\lambda_p$, full width at half maximum extinction of primary diffraction. λ^m_s, wavelength (nm, in air) for maximum extinction of secondary diffraction. H_s, maximum extinction of secondary diffraction. $\Delta\lambda_s$, full width at half maximum extinction of secondary diffraction.

~1.8. The Figure 1 CCA is in the intermediate thickness regime for the primary diffraction.

Table 3 compares the measured extinction spectrum to that calculated by DDT for three different CCA samples. The secondary diffraction extinction wavelength maxima predicted by DDT agree well with the measurements. In addition, the calculated primary diffraction extinction also agrees with that measured. We believe this is the first successful quantitative modeling of CCA primary diffraction extinction. The remaining discrepancy from theory probably results from crystal mosaicity and defects.

DDT[20] predicts for the thin or intermediate thickness crystal limit that the extinction bandwidth is inversely proportional to the effective crystal thickness, i.e. the number of lattice planes which contribute to the diffraction. For a fixed crystal thickness (t_0), the number of planes is proportional to $1/d_{hkl}$, and thus, to the reciprocal of the diffracted wavelength (λ). For the thick crystal limit, the extinction bandwidth is independent of the diffracted wavelength.[20]

Table 3 shows that the calculated primary diffraction bandwidth increases as the diffraction wavelength increases, as expected for the thin or intermediate thickness crystal regime. In contrast, the secondary diffraction bandwidth is almost independent of the diffracted wavelength. This is expected in the thick crystal regime. The thick crystal limit occurs due to the increased n_m for shorter wavelength, due to the superposition of Bragg diffraction from numerous lattice planes, and due to the decreased d_{hkl} which increases the number of planes.

The measured primary diffraction extinction bandwidth is relatively independent of the diffraction wavelength, which may indicate that the crystal orientation defects dominate the diffraction bandwidth.

The calculated secondary extinction maxima are ca. 4−10-fold larger than the measured values, while the bandwidths are ca. 4-fold smaller (Table 3). As discussed above, the increased secondary diffraction sensitivity to the crystal orientation and perfection may account for part of the increased discrepancy.

The DDT used here is not exact for secondary diffraction because it does not explicitly involve the simultaneous diffraction of multiple waves.[24] Our approximation assumes that only two waves exist in the crystal, i.e. one incident wave and one diffracted wave, and that the secondary diffraction extinction results from the independent diffraction by different lattice planes at the intensity level. We probably over estimate the maximum secondary diffraction extinction since diffraction theory should involve a summation at the electric field level.

Conclusions

We have observed an anomalously intense secondary diffraction, for incident light normal to the bcc (110) or fcc (111) planes. Bragg diffraction from numerous lattice planes are fortuitously superimposed for half the primary diffracted wavelength. This provides more than an order of magnitude higher diffraction efficiency. The diffracted wavelength can be continuously selected from deep in the UV into the visible region. This phenomenon may be useful for narrow band optical rejection filters for applications such as Raman spectroscopy, for pump-probe laser techniques,[8−12] and for applications in display technologies.

We have quantitatively modeled the primary and secondary diffraction of CCA using dynamical X-ray diffraction theory and light scattering theory. We find excellent agreement between the calculated and the measured extinction for the primary diffraction.